JOURNAL OF MATERIALS SCIENCE 30 (1995) 4380–4388

Toughening mechanisms for a zirconia–lithium aluminosilicate glass-ceramic

R. D. SARNO, M. TOMOZAWA
Rensselaer Polytechnic Institute, Department of Materials Engineering, Troy, New York

The mechanical properties of a lithium aluminosilicate glass-ceramic and the same glass-ceramic containing 5 and 15 wt% zirconia were investigated. The aim of the study was to assess the contributions to toughening from various toughening mechanisms. For the zirconia-containing compositions, zirconia initially precipitated, upon heat treatment of the glass, as tetragonal zirconia (t-ZrO_2), and upon further heat treatment, transformed to monoclinic zirconia (m-ZrO_2). This transformation could also be induced by grinding samples containing t-ZrO_2. By heat treating, the fracture toughness of all compositions increased with increasing matrix grain size until the matrix grain size exceeded ~ 1 μm, whereupon both the fracture toughness and strength decreased sharply. The matrix phases, lithium metasilicate and β-eucryptite, have either high thermal expansion mismatch or high thermal expansion anisotropy resulting in large thermal stresses. The initial toughness increases observed in each composition were attributed to the formation of a microcrack zone around the propagating crack. At larger grain sizes, thermal stresses caused spontaneous cracking and loss of strength. Zirconia additions also contributed to the fracture toughness improvement; however, the predominant toughening mechanism was not by transformation but due to crack deflection by the stress fields around the transformed, i.e. m-ZrO_2, particles.

1. Introduction

Glass-ceramics have a wide variety of useful and unique properties, and it is desirable to improve their toughness. Several methods have been successfully employed for toughening glass-ceramics. These include the formation of surface compressive stresses through ion exchange [1–3], fibre reinforcement using both brittle [4, 5] and ductile [6] fibres, and the addition of Ti particles to bioactive glass-ceramics [7]. Zirconia-toughened glass-ceramics have also been investigated [8–20] following toughness improvements realized in conventionally processed ceramics [21–25]. In this paper, details of the toughening mechanisms of zirconia-containing lithium aluminosilicate glass-ceramics were investigated.

2. Experimental procedure

2.1. Sample preparation

The composition $22.2Li_2O$–$18.9Al_2O_3$–$55.9SiO_2$ – $3.0P_2O_5$ (wt%) described by McMillian and Partridge [26] was chosen as the main glass to be investigated. The selection of this composition was based on its ability to dissolve an appreciable amount of zirconia. Glasses near the β-spodumene (Li_2O–Al_2O_3–$4SiO_2$) composition, which is the main crystalline phase in many commercial Li_2O–Al_2O_3–SiO_2 glass-ceramics, were unable to dissolve much more than 5 wt % ZrO_2. Earlier work by Watson [27] showed that the ZrO_2 solubility in alkali aluminosilicate melts increased with an increasing alkali/alumina ratio. The base glass composition in the present study has been reported [26] as one that will form a fine-grained glass-ceramic when given appropriate heat treatment. Using this base glass, the compositions listed in Table I, containing various amounts of ZrO_2, were prepared.

The raw materials used were Li_2CO_3, Al_2O_3, SiO_2 (Fisher Scientific, Springfield, NJ), $Al(PO_3)_3$ and either ZrO_2 or Li_2ZrO_3 (Alpha Products, Ward Hill, MA). Li_2ZrO_3 was used in preparing samples containing greater than 10 wt % zirconia. The powders were mixed by mechanically shaking for 45 min with an Impandex Inc. Type T2C Turbula Mixer (Impandex, Maywood, NJ) before melting in a 75 ml Pt–20% Rh covered crucible (Johnson Matthey, Inc., West Chester, PA) using a CM Rapid Temp Furnace Model 1700M (C.M. Inc., Bloomfield, NJ) equipped with a Eurotherm Analog Temperature Controller Model 912 (Eurotherm Corporation, Reston, VA) for 4 h at 1450–1600 °C. The exact temperature depended upon the ZrO_2 content of the glass. The melts were occasionally stirred with a SiO_2 (T08) glass rod. After melting, the glasses were poured onto a brass plate and annealed in a Thermolyne Model 2000 furnace (Barnstead/Thermolyne Corporation, Dubuque, IA) for 1 h and then furnace-cooled. Each melt was checked for homogeneity by examination with a Polarizing Instrument Co. Model 204 Polariscope

0022–2461

TABLE I Glass-ceramic compositions (wt %) and heat treatment schedule

	Li_2O	Al_2O_3	SiO_2	P_2O_5	ZrO_2
LAS0Z	22.2	18.9	55.9	3.0	0.0
LAS5Z	21.1	17.9	53.1	2.9	5.0
LAS15Z	18.9	16.1	47.5	2.5	15.0

Composition	Nucleation temperature (°C) (50 h)	Growth temperature (°C)	Growth time (h)
LAS0Z	485	955	6
			30
			75
			100
			150
LAS5Z	510	955	6
			75
			150
			200
LAS15Z	525	955	6
			75
			150
			300

(Polarizing Instrument Co., Inc., Irvington-on-Hudson, NY). If inhomogeneities were detected, the glass was crushed and remelted.

The proper nucleation temperature for each composition was determined by the method of Marotta *et al.* [28]. An initial DTA scan of quenched glass powder was run to determine the values of the glass transition temperature, T_g, and the crystallization peak temperature, T_P. Bulk samples of each glass were then given a 4-h heat treatment at a series of temperatures in 15 °C intervals in the approximate range $T_g - 45$°C to $T_g + 45$°C. A value of $1/T_P - 1/T_{P'}$, where $T_{P'}$ is the crystallization peak temperature of the quenched glass and T_P that of the heat-treated glass, is a measure of the nucleation rate.

DTA samples were prepared by crushing the glass with a mortar and pestle followed by sieving, so that the particle size used was between 246 and 417 μm. The sample weight was approximately 75 mg. The data were acquired at a scanning rate of 20 °C min^{-1} under an inert (N_2 or Ar) atmosphere with a Perkin-Elmer DTA 1700 furnace and a Perkin-Elmer 7/4 Thermal Analysis Controller (Perkin-Elmer, Norwalk, CN). The glass compositions were crystallized using a two-stage heat-treatment process. Each glass was nucleated for 50 h at the temperature of maximum nucleation rate. After nucleation, the glass was cut into rectangular bars, approximately 4 mm × 3 mm × 20 mm, using either a Buehler Isomet (Buehler Ltd., Evanston, IL) or a Leco VC-50 (Leco Corp., St. Joseph, MI) diamond wafering saw. These bars were then polished on each face using 240, 320, 400 and 600 grit SiC paper with water as a coolant. To ensure that opposite sample faces were parallel (a requirement for successful precracking of the specimens for fracture toughness measurements), the bars were then lapped using a Lapmaster International Model 12 Portable Precision Loose Abrasive Processing Machine (Lapmaster International, Morton Grove, IL) equipped with a diamond stopped fixture. A slurry of 1000 grit SiC in oil was the abrasive medium. A final polish with a CeO_2–water slurry on a felt pad was given to each face. The polished samples were then heated to the growth temperature of 955 °C and held at this temperature from 2 to 300 h to vary the m-/t-ZrO_2 ratio. A summary of heat treatments used in this study is also presented in Table I. After the appropriate time at the growth temperature, the samples were then furnace-cooled to room temperature. Both nucleation and crystal growth heat treatments were carried out in a Thermolyne Type 48000 Programmable Furnace (Barnstead/Thermolyne Corp., Irvington-on-Hudson, NY). The temperature was controlled by an R-type thermocouple positioned within 2 cm above the samples.

Crystal phase, per cent crystallinity, and the m-/(m- + t-ZrO_2) ratio were determined by X-ray diffraction. Bulk samples were used for both phase identification and the m-/(m- + t-ZrO_2) ratio; powdered samples were used for per cent crystallinity. X-ray diffraction data were collected using CuK_α radiation on either a Philips Model 5520 X-ray diffractometer (Philips Electronic Instruments Co., Mahwah, NJ) operated at 40 kV and 35 mA, or a Scintag XDS 2000 diffractometer (Scintag, Inc., Sunnyvale, CA) operated at 45 kV and 40 mA.

The method of Ohlberg and Strickler [29] was used to calculate the weight per cent crystallinity. The amount of t-ZrO_2 that has transformed to m-ZrO_2 was determined using the method of Toraya *et al.* [30]. Because grinding can induce the tetragonal to monoclinic transformation, the volume fraction measurements were determined from bulk specimens.

2.2. Fracture toughness

Fracture toughness was determined using the Single-Edge-Precrack-Beam (SEPB) [31] method in which

a precracked specimen was broken in oil using a three-point bending jig with a 16 mm span and an Instron Universal Testing Machine Model TT-D (Instron Corp., Canton, MA).

K_{IC} was then calculated from [32]

$$K_{IC} = \frac{PS}{BW^{3/2}} 3\left(\frac{a}{W}\right)^{1/2}\left[1.99 - \frac{a}{W}\left(1 - \frac{a}{W}\right) \times (2.15 - 3.93\frac{a}{W} + 2.7\left(\frac{a}{W}\right)^2\right]\Big/ 2\left(1 + 2\frac{a}{W}\right) \times \left(1 - \frac{a}{W}\right)^{3/2} \quad (1)$$

where

a = pop-in crack length
B = sample width
W = sample thickness
P = load at fracture
S = beam span

Equation 1 is valid over the range $0 < (a/W) < 1$.

Alternatively, the fracture toughness can be determined quickly and simply, but less accurately, by using a hardness indentation method [33–35]. The indentation method was used in this study as a means of verifying the trend of the fracture toughness values obtained by the SEPB method for selected samples. Nine indentations were made in oil for each sample. K_{IC} was calculated by [33]

$$K_{IC} = P/\pi^{3/2} \tan 68^\circ c^{3/2} \quad (2)$$

where

P = applied load
c = crack length

2.3. Fracture strength

Fracture strength was measured in three-point bending [36] using a bending jig with a span of 16 mm and a displacement rate of 0.020 in min^{-1}. To avoid any moisture-enhanced slow crack growth, samples were first coated in mineral oil before testing. At least five samples were tested for each heat-treatment condition.

2.4. Grain size

The grain size of the matrix crystalline phases was measured as a function of heat-treatment time. The line intercept method [37] was used to determine the average grain size from SEM micrographs of etched surfaces:

$$L_{3,\alpha} = V_\alpha L_T / N_\alpha \quad (3)$$

where

$L_{3,\alpha}$ = mean linear intercept of matrix phase α
V_α = volume fraction of matrix phase α
L_T = total line length
N_α = number of grains of matrix phase α intercepted

V_α was determined by the point counting method [37]. A JEOL JSM-840 scanning microscope (JEOL USA, Peabody, MA) was used to obtain all SEM micrographs.

3. Results

The volume per cent of crystalline phases present was $\geq 95\% \pm 5\%$ for samples of each composition, even after the shortest growth heat-treatment time listed in Table I. Therefore, any significant variation in properties with longer heat-treatment times is unlikely due to an increase in crystallinity of the samples.

For LAS0Z, lithium metasilicate (Li_2O–SiO_2) and β-eucryptite (Li_2O–Al_2O_3–$2SiO_2$) were the only crystalline phases present after each heat treatment. The relative proportion of these two phases did not change with treatment time as shown by the two diffraction patterns in Fig. 1a. For LAS5Z and LAS15Z, the phases identified were lithium metasilicate, β-eucryptite and t- and/or m-ZrO_2. Representative patterns are shown in Fig. 1b for LAS5Z and Fig. 1c for LAS15Z. The thermal transformation of t- to m-ZrO_2 due to coarsening of the t-ZrO_2 phase during the growth treatment at 955 °C for LAS15Z is shown in Fig. 2. The fraction of transformed, i.e. monoclinic, zirconia for LAS5Z and LAS15Z calculated from the X-ray integrated intensities of the m-ZrO_2 ($\bar{1}\,1\,1$) and (1 1 1) peaks and from the t-ZrO_2 (1 1 1) peak is plotted versus heat-treatment time in Fig. 3. The t- to m-ZrO_2

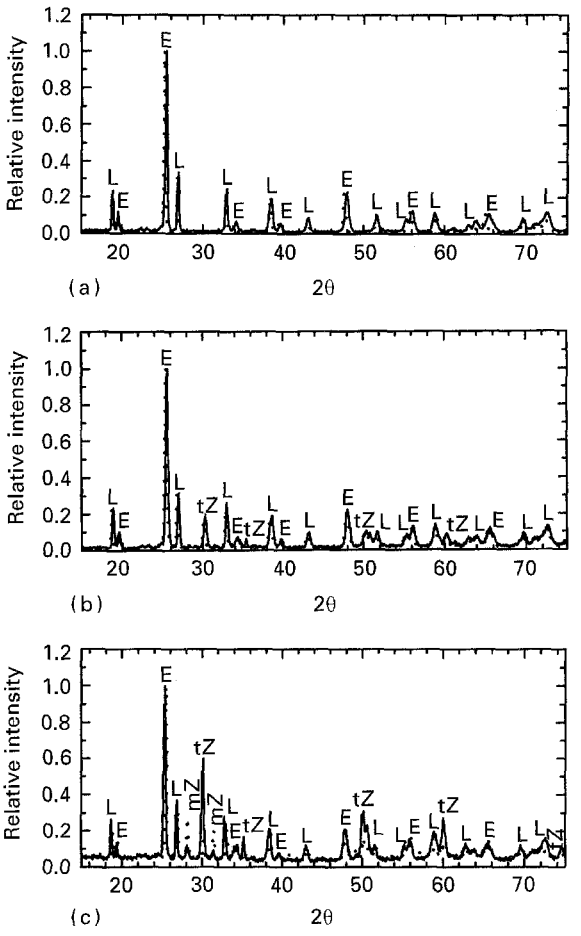

Figure 1 X-ray diffraction pattern after 6 h (solid line) and 150 h (dotted line) at 955 °C for (a) LAS0Z, (b) LAS5Z and (c) LAS15Z. L = lithium metasilicate, E = β-eucryptite, tZ = t-ZrO_2, and mZ = m-ZrO_2.

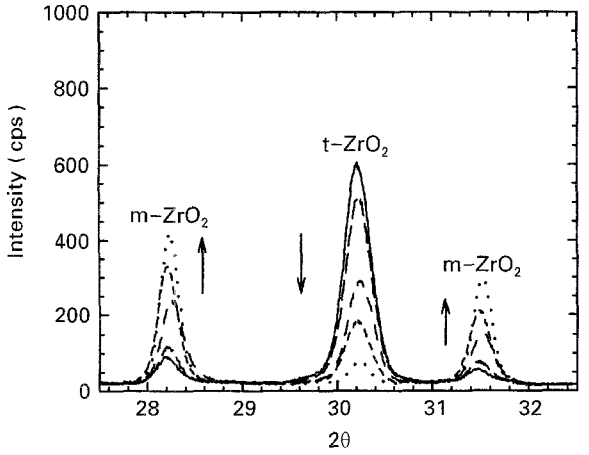

Figure 2 X-ray diffraction pattern of LAS15Z after various times showing the t- to m-ZrO_2 transformation with time at 955 °C. Arrow indicates increasing time. (—) 70 h, (— —) 140 h, (– –) 200 h, (– – –) 235 h, (···) 396 h.

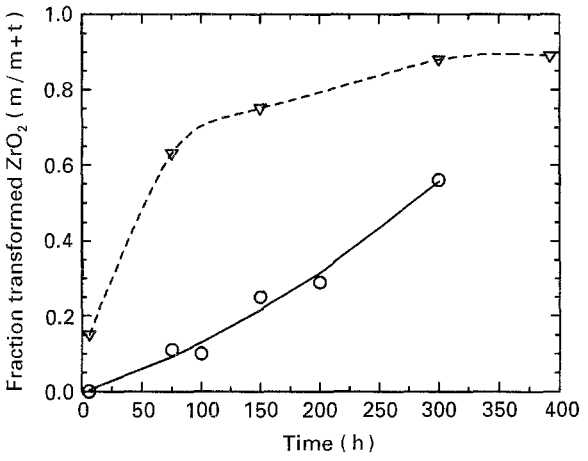

Figure 3 Fraction of transformed, i.e. monoclinic, ZrO_2, versus treatment time for LAS5Z and LAS15Z. (○) LAS5Z, (▽) LAS15Z.

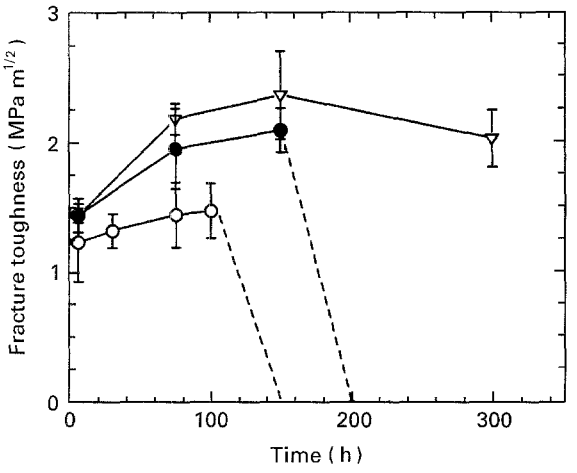

Figure 4 Room-temperature fracture toughness versus growth time at 955 °C for LAS0Z, LAS5Z and LAS15Z. (○) LAS0Z, (●) LAS5Z, (▽) LAS15Z.

transformation could also be stress-induced in this material by grinding a sample of LAS15Z to −400 mesh powder with a mortar and pestle.

Fig. 4 shows the fracture toughness measured by the SEPB method as a function of time at the 955 °C growth temperature for LAS0Z, LAS5Z and LAS15Z.

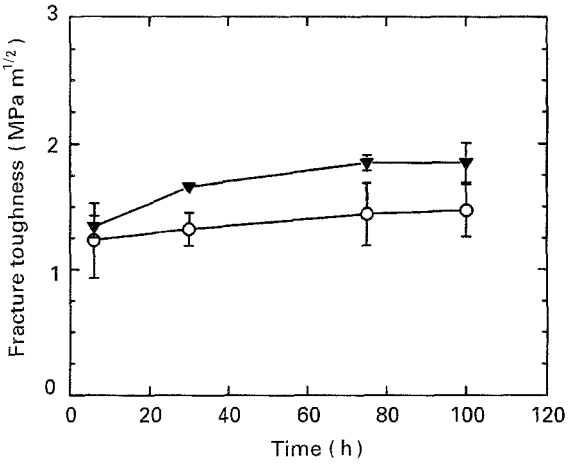

Figure 5 Room-temperature fracture toughness versus growth time at 955 °C for LAS0Z showing correlation of fracture toughness trend when measured by the SEPB and indentation methods. (○) SEPB, (▼) indentation.

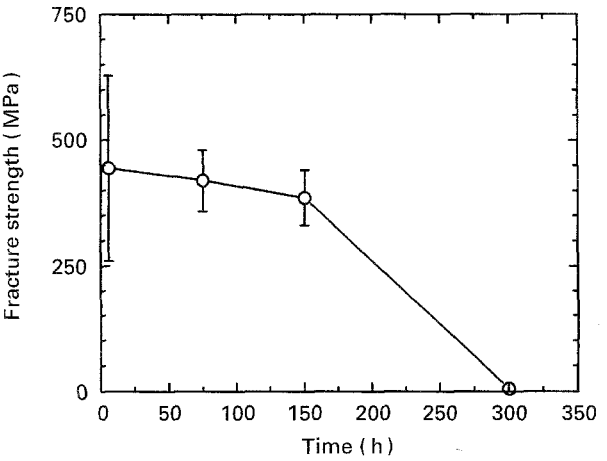

Figure 6 Room-temperatue fracture strength versus growth time for LAS15Z heat-treated at 955 °C.

The dashed lines for LAS0Z and LAS5Z indicate that spontaneous cracking occurred in the samples treated longer than 100 and 150 h, respectively.

K_{IC} measured by indentation for LAS0Z in comparison to that by the SEPB method is shown in Fig. 5. Fracture strength for LAS15Z is shown in Fig. 6.

4. Discussion

The fracture toughness shown in Fig. 4 increased steadily up to 100 or 150 h of growth time at 955 °C then dropped sharply. This decrease in K_{IC} is attributed to spontaneous cracking which occurs upon cooling to room temperature from the growth temperature due to thermal expansion anisotropy and/or mismatch between the two matrix phases. A large thermal expansion anisotropy exists between the a ($82.1 \times 10^{-7}\,K^{-1}$) and c ($-176 \times 10^{-7}\,K^{-1}$) directions for β-eucryptite and a large expansion mismatch exists between β-eucryptite (average $-90 \times 10^{-7}\,K^{-1}$) and lithium metasilicate ($148 \times 10^{-7}\,K^{-1}$). When the fracture toughness is replotted versus grain size in Fig. 7, it appears that once a critical grain size of ~1.0 μm is exceeded, spontaneous cracking occurs.

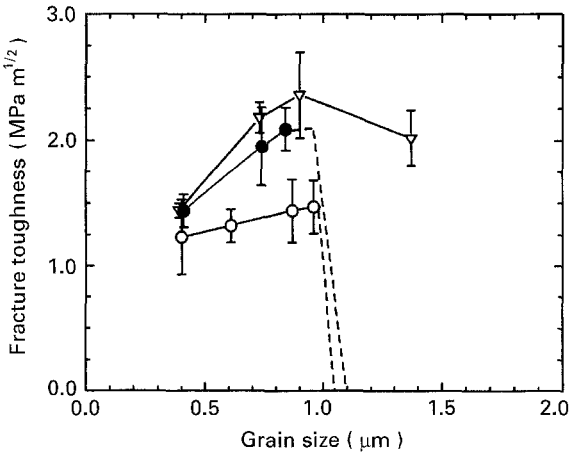

Figure 7 Room-temperature fracture toughness versus grain size after heat treatment at 955 °C for (○) LAS0Z, (●) LAS5Z and (▽) LAS15Z.

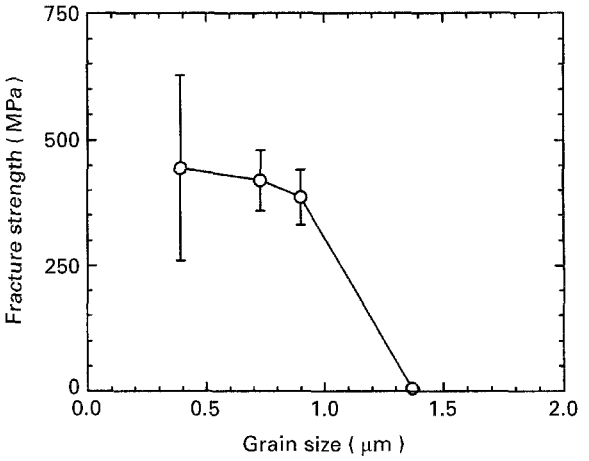

Figure 8 Room-temperature fracture strength versus grain size for LAS15Z heat-treated at 955 °C.

Spontaneous cracking in LAS0Z and LAS5Z occurs to the extent that extensive crack linking takes place. For the LAS15Z composition this crack linking was not as extensive as evidenced by the fact that LAS15Z samples with matrix grain size of 1.37 μm, although weakened, still possess some strength. The LAS0Z and LAS5Z samples with matrix grain size ~1.1 μm exhibit no residual strength at all. The decrease in K_{IC} for the 1.37 μm matrix grain size samples of the LAS15Z composition is thought to be due to microcrack formation prior to mechanical testing from the above-mentioned thermal stresses. Examination of Fig. 1a–c indicate that there is no difference in the lithium metasilicate to β-eucryptite ratio amongst these compositions.

A possible explanation for LAS15Z having 1.37 μm grain-size samples retaining some fracture toughness is that the ZrO_2 grains act as impediments to microcrack extension by arresting these cracks, thereby limiting crack linkage. The higher ZrO_2 content of the LAS15Z composition makes this mechanism more effective compared to LAS5Z.

The fracture strength of LAS15Z was determined after heat treatments at 955 °C. Fig. 8 shows the fracture strength versus grain size for this composition. Again, once a mean matrix grain size of ~1 μm is exceeded, the fracture strength is sharply degraded by thermal stress-induced microcracking upon cooling from the process temperature. Before this size is reached, the fracture strength is nearly constant. This suggests that microcrack formation as a result of the t- to m-ZrO_2 transformation prior to mechanical testing is not occurring. If prior microcracking had occurred, a decrease in strength would have been observed. Microcrack formation *during* mechanical testing as a form of toughening will be discussed.

In order to explain the observed variation in fracture toughness shown in Fig. 4, various toughening mechanisms relevant to the present system will be briefly reviewed.

4.1. Transformation toughening

An expression for transformation toughening has been derived by McMeeking and Evans [38] and by Budiansky *et al.* [39] for the incremental increase in fracture toughness, ΔK_{IC}, due to transformation toughening:

$$\Delta K_{IC} = AEV_f e^T h^{1/2} \quad (4)$$

where

A = constant $\leqslant 0.55$
E = Young's Modulus of the matrix
V_f = volume fraction of transformable t-ZrO_2
e^T = transformation strain
h = transformation zone height

Becher *et al.* [40–42] derived from Equation 4:

$$\Delta K_{IC} = AB^{1/2}(e^T)^2 V_f E K_{IC}^M / \Delta S(T - M_s) \quad (5)$$

where

ΔS = entropy change
K_{IC}^M = fracture toughness of the matrix
$B = [2(1 + \nu)^2/9\pi]$
γ = Poissons ratio

which shows the dependence of the toughness increment on the test temperature, T, and the spontaneous t- to m-ZrO_2 transformation temperature, M_s. It is important to note that in order to obtain appreciable toughening through the transformation toughening mechanism, it is not sufficient to have only a large volume fraction of t-ZrO_2. This must be accompanied by an M_s temperature slightly below the test temperature.

4.2. Microcracking toughening

Rice and Freiman [43] derived a theoretical expression relating the increase in fracture energy, γ, to grain size, g, when microcracking is induced by thermal expansion anisotropy for noncubic materials. From strain-energy arguments, the total fracture energy of a material, γ, was given by [43]

$$\gamma = \gamma_{pc}(1 - g/g_s) + M\Delta e[(9E\gamma_B g)^{1/2} - \Delta e E g] \quad (6)$$

where

γ_{pc} = polycrystalline surface energy
g = grain size
g_s = grain size for spontaneous microcracking
M = constant between 1 and 3

γ_B = average grain-boundary fracture energy
$\Delta e = \Delta\alpha\Delta T$
$\Delta\alpha$ = r.m.s. thermal expansion mismatch

Both the model for microcracking associated with phase transformations and the model of Rice and Freiman. assume a microcrack zone forms with the propagating crack in the absence of any pre-existing, spontaneously formed microcracking.

4.3. Crack deflection toughening

A propagating crack which encounters either fracture-resistant second-phase particles or localized residual stress fields, can be deflected out of the plane normal to the applied tensile stress. When this occurs, loading is no longer mode I. A mixed-mode analysis is required in which the components of K for each mode are calculated and then combined with a mixed-mode failure criterion. The net effect of crack deflection is to reduce the crack extension force on the deflected segment. Faber and Evans [44] have developed theoretical models to predict the relative toughness increase due to crack deflection from particles of various shapes. Zirconia particles precipitated in glass or glass-ceramics are generally spherical in shape [8, 45]. Toughening by this mechanism is expected to be independent of temperature and particle size. However, if deflection is affected by residual stresses resulting from thermal expansion differences, some temperature sensitivity may result [25].

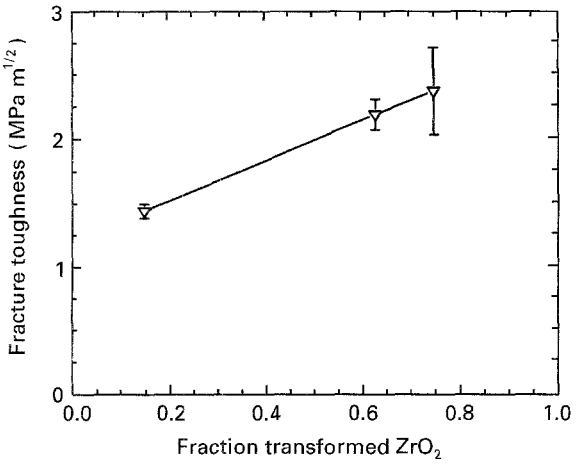

Figure 9 Room-temperature fracture toughness versus fraction of transformed zirconia for LAS15Z.

Improvement in the fracture toughness from transformation toughening does not seem to be a factor in this system. Fig. 9 shows the fracture toughness versus the transformed ZrO_2 fraction. The fracture toughness is actually observed to *increase* as the amount of transformable t-ZrO_2 *decreases*, contrary to the trend predicted for transformation toughening by Equation 4. The incremental increase in fracture toughness, ΔK_{IC}, due to transformation toughening can be estimated using either Equation 4 or 5. Equation 5 relates the fracture toughness improvement to the martensitic start temperature, M_s. From X-ray diffraction studies of quenched samples, it can be stated that the M_s temperature for the untransformed t-ZrO_2 remaining after each heat treatment in the LAS15Z composition is lower than the liquid nitrogen temperature, $-196\,^{\circ}C$.

The M_s temperature can be used to calculate the critical transformation stress [40], $\sigma_c^T = (T - M_s) \times \Delta S/e^T$. Using values for the transformation strain, e^T, of 0.04 [25] and for the entropy of transformation, ΔS, of 150×10^3 Pa K^{-1} [40], σ_c^T is 828.75 MPa for LAS15Z. Calculation of ΔK_{IC} for the optimally toughened LAS15Z composition by Equation 5 gives a value of only 0.05 MPa m$^{1/2}$, and by Equation 4, 0.06 MPa m$^{1/2}$. A value of 0.1 μm for the transformation zone height, h, calculated from [40] $h = B(K_{IC}^M/\sigma_c^T)^2$ was used in Equation 4.

The increase in room temperature fracture toughness with increasing grain size and increasing total ZrO_2 content, as seen in Fig. 4 for the three compositions studied, can be attributed to two predominant toughening mechanisms, microcrack toughening and toughening by crack deflection. Direct microscopic evidence exists for both of these processes. The microcrack toughening process is active in all three compositions, whereas crack deflection takes place only in the ZrO_2-containing LAS5Z and LAS15Z compositions.

Fig. 10a and b are SEM micrographs of LAS0Z and LAS15Z which were each given a 115 h growth treatment at 955 °C. Both samples were polished with CeO_2 after heat treatment, then indented with a Vickers hardness indenter using a 10 kg load. For

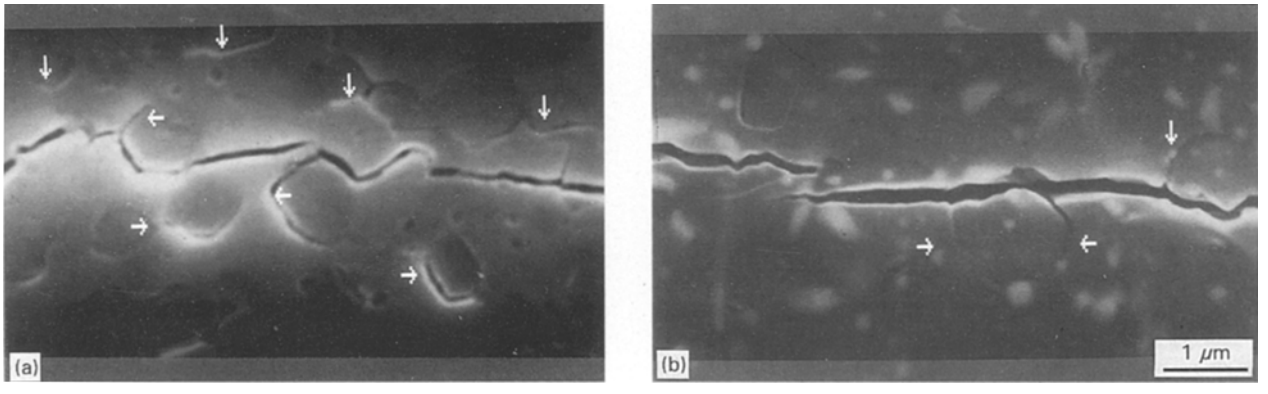

Figure 10 SEM micrograph of (a) LAS0Z and (b) LAS15Z, after 115 h at 955 °C. Arrows show microcracks.

both samples, microcracks formed around the main crack generated by Vickers indentation. The mean grain size of the LAS0Z sample is greater than that for the LAS15Z sample. This results in the formation of a larger microcrack zone during propagation of the indentation crack. In addition, after this heat treatment, X-ray diffraction analysis for LAS15Z showed that most of the ZrO_2 (light grey phase) had transformed to the monoclinic phase. No microcracking due to the volume expansion of the t- to m-transformation is observed, as has been reported elsewhere [46,47]. Transformation microcracking would also have caused a reduction in the measured fracture strength, which was not observed.

The fracture energy, $\gamma = K_{IC}^2/2E$, was determined to be 1.47 ± 0.21 MPa $m^{1/2}$ for the optimally toughened LAS0Z, while Equation 6 predicts 1.45 MPa $m^{1/2}$. In this equation, the polycrystalline fracture energy, γ_{pc}, was determined from the measured fracture toughness of LAS0Z with a small average matrix grain size of < 0.1 μm Therefore, no appreciable contribution from microcrack toughening is expected for this sample. The sample was prepared by a 48-h nucleation heat treatment at 485 °C and a 10-h growth treatment at 825 °C. The fracture toughness of this material was 1.18 MPa $m^{1/2}$ which corresponds to a fracture energy, γ_{pc}, of 6.32 J m^{-2}. Using a grain size for spontaneous cracking, g_s, of 1.10 μm, and a grain boundary fracture energy, γ_B, of 5.14 J m^{-2} calculated from [44]

$$\gamma_B = g_s(\Delta e E)^2/12E(1 - \nu) \quad (7)$$

the total fracture energy for LAS0Z calculated by Equation 6 was 9.50 J m^{-2}. This corresponds to a fracture toughness of 1.45 MPa $m^{1/2}$ which agrees well with the measured value, indicating that microcrack toughening is the dominant toughening mechanism.

The greater toughness improvement realized by the LAS5Z and LAS15Z compositions over LAS0Z is due to the additional mechanism of crack deflection for these materials. In this case, the crack is considered to be deflected by the stress fields around transformed, monoclinic, zirconia particles. Evidence for this is shown in Figs 11 and 12 which are SEM micrographs of the surface near cracks generated by Vickers indentation. Fig. 11 is for samples of LAS15Z, which were heat-treated at 955 °C for 2–200 h. With increasing treatment time, the fraction of transformed, monoclinic, zirconia increases. Fig. 11 a–d corresponds to samples that have 0.0, 0.27, 0.55 and 0.77 volume fraction, respectively, of the zirconia transformed to the monoclinic phase. The crack shows increased deflection with greater m-ZrO_2 content.

In comparison, Fig. 12 is for LAS0Z samples also given heat treatments at 955 °C for 30, 75 and 100 h. Here, no deflection of the Vickers crack is observed. The matrix grain sizes of LAS0Z in Fig. 12a–c are 0.61, 0.87 and 0.96 μm, respectively, comparable to the matrix grain sizes of LAS15Z in Fig. 11b–d of 0.39, 0.73 and 0.90 μm, respectively, indicating that deflection must be from the transformed, i.e. monoclinic, ZrO_2 particles and not due to coarsening of the matrix.

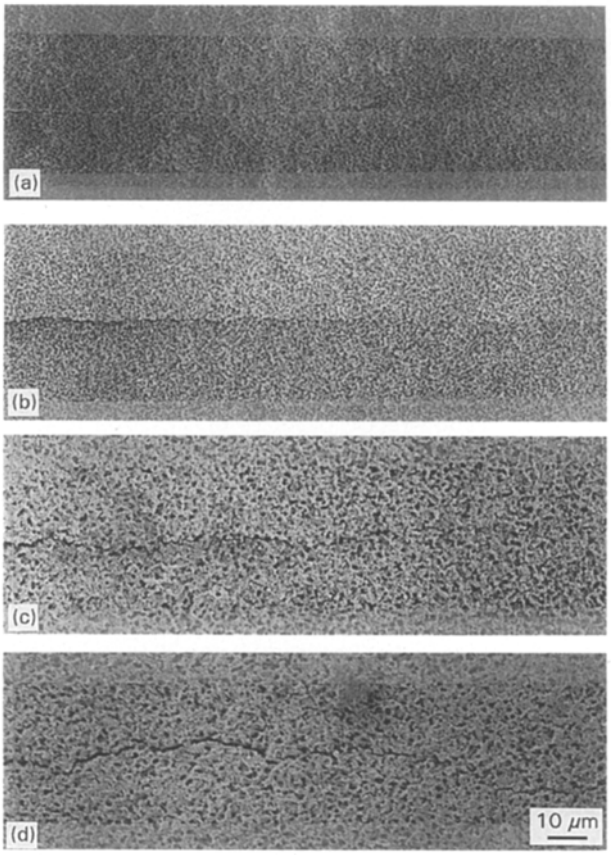

Figure 11 Deflection of a Vickers crack in LAS15Z by m-ZrO_2 particles. Crack deflection increases with the amount of transformed ZrO_2; (a) 0.0; (b) 0.27; (c) 0.55; (d) 0.77 volume fraction of transformed ZrO_2. Crack propagation is from left to right.

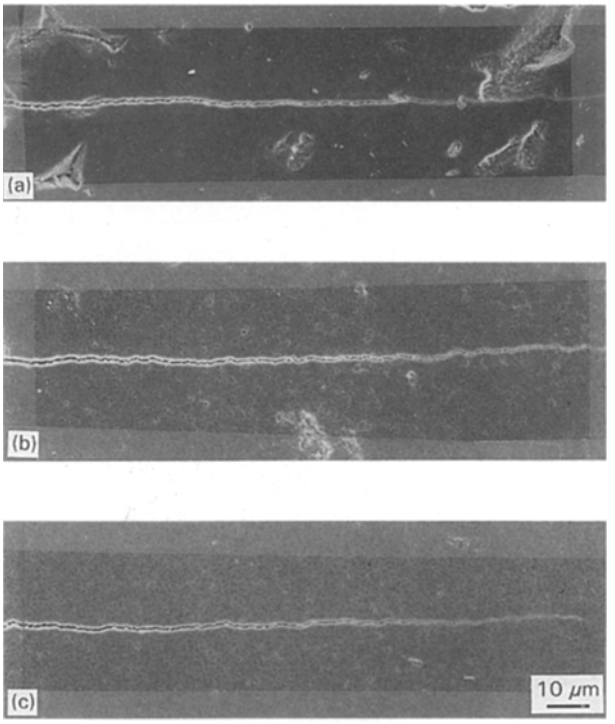

Figure 12 No deflection of a Vickers crack in LAS0Z which was heat-treated at 955 °C for (a) 30, (b) 75 and (c) 100 h. Crack propagation is from left to right.

The amount of toughening from crack deflection can be estimated from the theory of Faber and Evans. From their plots of the calculated relative toughness [44], K_{IC}/K_{IC}°, versus volume fraction of deflecting

TABLE II Comparison of predicted and measured K_{IC}/K_{IC}° for LAS5Z and LAS15Z

	K_{IC}/K_{IC}°
LAS15Z 955 °C growth temperature	
Predicted	1.38
Measured	1.45
LAS5Z 955 °C growth temperature	
Predicted	1.25
Measured	1.28

particles, where K_{IC}° is the fracture toughness of the material with no crack deflection, the expected toughness improvement from crack deflection can be obtained. Since deflection in this situation is from the stress fields around transformed zirconia particles, an effective stress field radius of 2.5 times the particle radius was used to determine the volume fraction. Assuming that the amount of microcrack toughening in the LAS5Z and LAS15Z compositions is the same as for LAS0Z, the observed maximum fracture toughness improvement for these two materials can be accounted for by the combined effect of microcrack toughening and crack deflection toughening. Table II lists the observed and predicted fracture toughness due only to crack deflection for these cases.

5. Conclusions

As a result of the present research the following conclusions can be made.

1. Transformation toughening is not a major contributor to the improved fracture toughness of the LAS5Z or LAS15Z composition.
2. Microcrack formation due to residual thermal expansion mismatch stresses between lithium metasilicate and β-eucryptite during mechanical testing leads to microcrack toughening, which is the dominant toughening mechanism in the LAS0Z composition.
3. The critical matrix grain size for spontaneous cracking is ~ 1 μm. Once this grain size is exceeded, both the fracture toughness and fracture strength drop off sharply.
4. Additions of ZrO_2 enhance the fracture toughness by causing crack deflection from stress fields around transformed, m-ZrO_2, particles, and crack deflection is the dominant toughening mechanism for the LAS5Z and LAS15Z compositions.
5. No matrix microcracks were observed to form by the t- to m-ZrO_2 transformation so the transformation stresses were fully retained.

Acknowledgement

This research was supported by the US Army Research Office under Grant No. DAAL 03-91-4-0211.

References

1. B.R. KARSETTER and R.O. VOSS, *J. Am. Ceram. Soc.* **50** (3) (1967) 133.
2. G.H. BEALL, B.R. KARSETTER and H.L. RITTER, *ibid.* **50** (4) (1967) 181.
3. D.A. DUKE, J.F. MAC DOWELL and B.R. KARSETTER, *ibid.* **50** (2) (1967) 67.
4. J. AVESTON, in "The properties of Fibre composites" (IPC Science and Technology Press, London, 1972).
5. R.A.J. SAMBELL, D.H. BOWEN and D.C. PHILLIPS, *J. Mater. Sci.* **7** (6) (1972) 663.
6. *Idem., ibid.* **7** (6) (1972) 676.
7. T.B. TROCZYNSKI and P.S. NICHLOSON, *J. Am. Ceram. Soc.* **74** (8) (1991) 1803.
8. D.R. CLARKE and B. SCHWARTZ, *J. Mater. Res.* **2** (6) (1987) 801.
9. M.A. McCOY and A.H. HEUER, *J. Am. Ceram. Soc.* **71** (8) (1988) 673.
10. C.A. SORRELL and C.C. SORRELL, *ibid.* **60** (11–12) (1977) 495.
11. G. FAGHERAZZI, S. ENZO, V. GOTTARDI and G. SCARINCI, *J. Mater. Sci.* **15** (11) (1980) 2693.
12. B.H. MUSSLER, and M.W. SHAFER, *Am. Ceram. Soc. Bull.* **64** (11) (1985) 1459.
13. M. NOGAMI and M. TOMOZAWA, *J. Am. Ceram. Soc.* **69** (2) (1986) 99.
14. K.D. KEEFER and T.A. MICHALSKE, *ibid.* **70** (4) (1987) 227.
15. G. LEATHERMAN and M. TOMOZAWA, *J. Mater. Sci.* **25** (1990) 4488.
16. M. NOGAMI, K. NAGASAKA, K. KADONO and T. KISHIMOTO, *J. Non-Cryst. Solids* **100** (1988) 298.
17. Y. CHENG and D.P. THOMPSON, *Br. Ceram. Trans. J.* **87** (3) (1988) 107.
18. *Idem. J. Mater. Sci. Lett.* **9** (1) (1990) 24.
19. S. SRIDHARAN and M. TOMOZAWA, *J. Non-Cryst. Solids* **182** (1995) 262.
20. C.T. REED, M.J. HAUN, T.K. BROG, K.R. McNERNEY, J.D. SIBALD and D.G. WIRTH, in Proceedings of the Ceramic Matrix Composites Symposium of the 1993 American Ceramic Society Annual Meeting, to be published.
21. A.H. HEUER and L.W. HOBBS (eds), "Advances in Ceramics", Vol. 3 (American Ceramic Society, Columbus, Ohio, 1981).
22. N. CLAUSSEN, M. RUHLE and A.H. HEUER (eds), "Advances in Ceramics", Vol. 12 (American Ceramic Society, Columbus, Ohio, 1984).
23. S. SOMIYA, N. YAMAMOTO and H. YANAGIDA (eds), "Advances in Ceramics", Vol. 24 (American Ceramic Society, Westerville, Ohio, 1988).
24. E.H. LUTZ and N. CLAUSSEN, *J. Am. Ceram. Soc.* **74** (1) (1991) 11.
25. D.J. GREEN, R.H.J. HANNINK and M.V. SWAIN, "Transformation Toughening of Ceramics" (CRC Press, Inc., Boca Raton, FL, 1989).
26. P.W. McMILLIAN and G. PARTRIDGE, British Patent 924 996 (1963).
27. E.B. WATSON, *Contrib. Mineral. Petreol.* **70** (1979) 407.
28. A. MAROTTA, A. BURI and F. BRANDA, *J. Mater. Sci.* **16** (2) (1981) 341.
29. S.M. OHLBERG and D.W. STRICKLER, *J. Amer. Soc.* **45** (4) (1962) 170.
30. H. TORAYA, M. YOSHIMURA and S. SOMIYA, *J. Am. Ceram. Soc.* **67** (6) (1984) C119.
31. T. NOSE and T. FUJII, *ibid.* **71** (5) (1988) 328.
32. D. BROEK, "Elementary Fracture Mechanics" (Martinus Nijhoff, Boston, 1987) p. 181.
33. C.B. PONTON and R. D. RAWLINGS, *Mater. Sci. and Technol.* **5** (9) (1989) 865.
34. *Idem. ibid.* **5** (10) (1989) 961.
35. M.-O. GUILLOU, J.L. HENSHALL, R.M. HOOPER and G.M. CARTER, *J. Hard Mat.* **3** (3–4) (1992) 421.
36. F.P. BEER and E.R. JOHNSTON Jr, "Mechanics of Materials" (McGraw-Hill, Inc., New York, 1981) p. 589.
37. G.F. VANDER VOORT, "Metallography – Principles and Practices", (McGraw-Hill Book Co., New York, 1984) p. 423.
38. R.M. McMEEKING and A.G. EVANS, *J. Amer. Ceram. Soc.* **65** (5) (1982) 242.

39. B. BUDIANSKY, J.W. HUTCHENSON and J.C. LAMBROPOULOS, *Int. J. Solids Struct.* **19** (4) (1983) 337.
40. P.F. BECHER, M.V. SWAIN and M.K. FERBER, *J. Mater. Sci.* **22** (1) (1987) 76.
41. P.F. BECHER and M.V. SWAIN, *J. Am. Ceram. Soc.* **75** (3) (1992) 493.
42. P.F. BECHER, K.B. ALEXANDER, A. BLEIER, S.B. WATERS and W.H. WARWICK, *ibid.* **76** (3) (1993) 657.
43. R.W. RICE and S.W. FREIMAN, *ibid.* **64** (6) (1981) 350.
44. K.T. FABER and A.G. EVANS, *Acta Metall.* **31** (4) (1983) 565.
45. G. LEATHERMAN, PhD Thesis, R.P.I., Troy, New York (1986).
46. H. RUF and A.G. EVANS, *J. Am. Ceram. Soc.* **66** (5) (1983) 328.
47. N. CLAUSSEN, *ibid.* **59** (1–2) (1976) 49.

Received 4 July 1994
and accepted 9 January 1995